

# Role of Protonation State and Solvation on the pH Dependent Optical Properties of Bromocresol Green

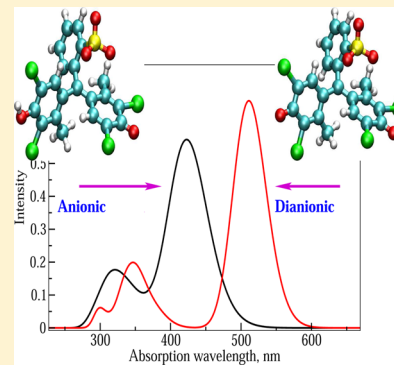
N. Arul Murugan,<sup>\*,†</sup> Sigurd Schrader,<sup>‡</sup> and Hans Ågren<sup>†</sup>

<sup>†</sup>Division of Theoretical Chemistry and Biology, School of Biotechnology, Royal Institute of Technology, SE-10691 Stockholm, Sweden

<sup>‡</sup>Technische Hochschule Wildau, Hochschulring 1, 15745 Wildau, Brandenburg, Germany

## Supporting Information

**ABSTRACT:** pH sensors play a key role in many industrial and diagnostic applications. Mostly their usage is based on experience, and in many cases the working mechanisms of these sensors are not known in detail, thereby hindering a systematic improvement of such sensors for specific applications. In this report, we present results from combined quantum chemical and molecular mechanics calculations of molecular structures and optical absorption properties of bromocresol green (BRG) in aqueous solution with varying pH value. In the acidic pH range, this chromophore has an intense band with absorption maximum at 444 nm and in the basic pH regime the absorption spectra show a redshift toward 613 nm. In order to identify the molecular structures responsible for this pH dependent optical behavior the closed and open forms of BRG are studied using static approaches considering in each case the three possible protonated states namely, neutral, anionic, and dianionic. For the most significant forms, i.e. the open forms of BRG, extensive modeling based on the integrated approach has been carried out, where the structure and dynamics were studied using hybrid QM/MM molecular dynamics, while the excitation energy calculations were carried out using time dependent density functional theory wherein the surrounding solvent was described as polarizable continuum, semicontinuum, or via a molecular mechanics force-field. The anionic and dianionic forms of BRG have been recognized as molecular forms responsible for its acidic and basic pH behavior, respectively. In contrast to the case of solvatochromic probes, the different protonation states determine the optical behavior in different pH values for pH probes. Hence, the level of solvent description appears to be of minor importance. Independent of the level of theory used to describe the solvent, all models reproduce the spectral features of BRG in different pH and also the pH induced redshift in good agreement with experiment.



## 1. INTRODUCTION

pH sensitive molecular probes<sup>1,2</sup> have attracted considerable interest owing to their potential and practical use as sensors in biomedical, environmental, and industrial applications.<sup>3–5</sup> In the former area they fulfill an important mission in that a number of diseases are strongly associated with pH changes, and a secure and noninvasive sensing of the pH by designed<sup>6</sup> or natural probes<sup>7</sup> becomes, therefore, an important task. Gastroesophageal reflux disease and cancer are diseases that are associated with deviations from normal intracellular or extracellular pH,<sup>8–10</sup> to mention only a few. In addition to such direct connection, pH changes can play an indirect role such as stabilizing non-native structures of enzymes which are the functional units of the human body and might lead to a number of diseases. The pH dependent stabilization of  $\alpha$  or  $\beta$  secondary structures has been studied in detail for a number of peptides<sup>11</sup> and proteins such as human serum albumin.<sup>12</sup> The normal folding pathway of proteins to native states (which are their functional forms) of amyloid proteins are known to be perturbed by pH changes and may lead to misfolding and subsequently to the so-called conformational disease, Alzheimers disease.<sup>13</sup> Moreover, a number of body organelles like

lysosome and mitochondria are required to be in appropriate pH for normal functioning.<sup>14</sup>

The use of pH sensors in industrial applications deals with the monitoring of pH within reactors which is directly related to the control of reaction conditions or the corrosion of reactor components and so to their efficiency. pH-sensors are also used in water treatment, food processing units, and bioreactors.<sup>15</sup> The basic principles of optical pH detection usually rely on the pH dependent shifts of absorption and/or fluorescence of organic chromophores<sup>1,2</sup> or in more recent years also of highly luminescent semiconductor nanoparticles, quantum dots<sup>16,17</sup> incorporated into the active part of such sensors. Bromocresol green (BRG) or bromocresol purple indicator dyes dispersed in polymer matrices are currently used for pH sensing, and they are perhaps the most important examples of such pH sensing optical probes.

The present contribution relies on the so-called integrated approach in modern molecular modeling, i.e. on the combination of structural dynamics and multiscale modeling

Received: April 30, 2014

Published: August 8, 2014



ACS Publications

© 2014 American Chemical Society

3958

dx.doi.org/10.1021/ct500375x | J. Chem. Theory Comput. 2014, 10, 3958–3968

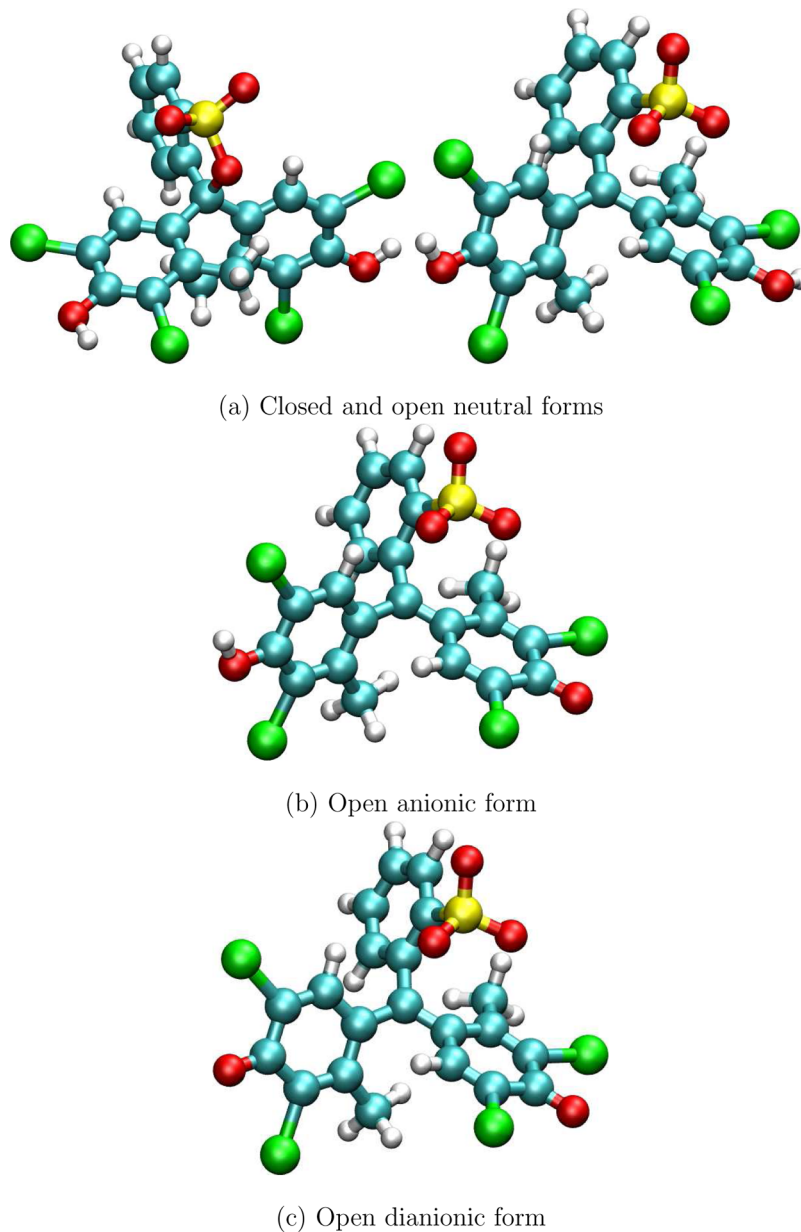


**Figure 1.** Molecular structure of the closed-neutral, open-neutral, open-anionic, and open-dianionic forms.

of properties and spectra. This approach provides a realistic proposition for design of pH indicators starting from basic principles. The precise interactions between medium and chromophores are then taken into account in a self-consistent fashion to build-up their optical response. Thus, various properties of surrounding media can be monitored by the probe in this way. Although the direct simulation of pH values in a given solution is still an arduous task, the pH sensing through specially designed probes can be feasible; in particular the effect of protonation of various sites should be within reach. In order to test this notion and to explore the capacity of current modeling in this respect, we address the important pH sensing optical dye, namely the aforementioned bromocresol green indicator, and study how modeling can reproduce its pH sensitive optical signal.

Bromocresol green (BRG) belongs to triphenylmethane type dye molecules. It can exist in a closed form, characterized by a central carbon atom in the  $sp^3$  hybridization state, and in open

forms where the central carbon (the carbon to which three phenyl rings are connected) is  $sp^2$  hybridized (see Figures 1a and 1b). Moreover, each of these forms can exist in a neutral, anionic, and dianionic molecular structure. So the former set differs with respect to hybridization of the central carbon, while the latter forms differ with respect to their protonation states. Usually, the pH dependent optical behavior is attributed to the pH dependent stabilization of different protonation states of the sensing molecule. Even different hybridization of the carbon in closed, and open forms can be attributed to a color change which is commonly observed in thermochromic or photochromic systems<sup>18</sup> where heat or light is involved in switching the hybridization. The  $sp^3 \Rightarrow sp^2$  transition leads to increased conjugation, and so the spectra of the open forms are redshifted in these systems. Therefore, it becomes essential to study all six molecular forms to understand which of the forms contribute to the pH dependence of the optical properties in these sensors.

Modeling the pH effect in the chromophore-solvent and bioenvironment subsystems is a computationally challenging task due to the complexity associated with the description of the concentration of protons/or hydroxyl ions in aqueous solution and the dynamic nature of hydrogen bond formation and breaking between the solute and the hydronium/hydroxyl ions in the solution. There exist static and dynamic approaches in the literature which treat the protonation states of acids,<sup>19–21</sup> organic molecules,<sup>22</sup> chromophore,<sup>23</sup> or peptides and proteins in a fixed way or time-dependently. In particular, the acidostat method and constant-pH simulations can be used to dynamically treat the protonation states.<sup>24</sup> Due to the unavailability of suitable implementation in the most commonly used molecular dynamics softwares, there are only a few studies using dynamical treatment of protonation states.<sup>24</sup> The static approaches for treating the protonation states are popular and routinely used in modeling the pH effect in the amino acid residues of proteins or chromophores.<sup>25,26</sup> In particular, the optical properties of a number of pH sensitive green fluorescent proteins where the chromophore and proteins can have varying protonation states depending upon the pH of the medium have been modeled successfully using the static approaches.<sup>27,28</sup> In this study we also employ a static approach to treat the pH effect on the BRG chromophore. Since it is not clear whether a single ionic form (namely neutral, anionic, or dianionic forms) or a mixture of these forms is responsible for the optical behavior in the given range of pH, we have studied all three forms in both open and closed states individually. We explore the optical properties using the static approach for all these six forms, and further extensive calculations using the integrated approach have been carried out for the three most relevant forms of BRG (open neutral, open anionic, and open dianionic). The integrated approach incorporates hybrid QM/MM molecular dynamics to model the structure of BRG in water as solvent at finite temperature. For the calculations of excitation energy we employed linear response time dependent density functional theory with the environment described using various approaches being namely (i) the polarizable continuum model,<sup>29</sup> (ii) the semicontinuum model,<sup>30</sup> and (iii) polarizable electronic embedding scheme.<sup>31,32</sup> The complexity and accuracy in the description of the medium effect increase from the former to the latter.

It is notable that T. D. Meyer et al.<sup>33</sup> recently studied the substituent effect on the optical properties of anionic and dianionic forms of sulfonaphthaline dyes experimentally and by employing density functional theory calculations using the B3LYP functional including BRG which is the candidate molecule in the present study. Their studies were limited to open anionic and dianionic forms of BRG and employed an implicit solvation model. In the current study we have scanned closed and open forms of BRG, and in addition we have considered all three possibilities for the protonation/deprotonation states (namely neutral, anionic, and dianionic which are referred to as  $\text{BRG}^0$ ,  $\text{BRG}^-$ , and  $\text{BRG}^{2-}$ ). Moreover we employ an explicit description of environment and account for the solvent-dependent structure of the ionic forms of BRG. We further consider the finite temperature and finite pressure effects by carrying out force-field and ab initio molecular dynamics simulations for BRG in solvent. Our main objective is to address the relative importance of the protonation states and solvation effect on the pH dependent optical properties of BRG using different approaches to describe the solvent in the excitation energies calculations. Below, we briefly outline the

two computational approaches employed to carry out static and dynamic calculations of one-photon absorption properties.

## 2. COMPUTATIONAL DETAILS

**2.1. Structure Modeling.** The structure modeling for three forms of BRG (i.e.,  $\text{BRG}^0$ ,  $\text{BRG}^-$ , and  $\text{BRG}^{2-}$ ) has been carried out by using force-field and ab initio molecular dynamics (MD). First, the molecular geometry of  $\text{BRG}^0$ ,  $\text{BRG}^-$ , and  $\text{BRG}^{2-}$  in both closed and open conformations were optimized using the B3LYP/6-311+G(d,p) method in water solvent which is described as a polarizable continuum using Gaussian09 software.<sup>34</sup> The cavity for the solute BRG molecule in the geometry optimization within solvent media is based on the UAHF parameter set.<sup>35</sup> Furthermore, the electrostatic potential fitted charges for the solute were obtained using the CHELPG procedure<sup>36</sup> as implemented in the Gaussian09 software. The optimized molecular geometry and the electrostatic potential fitted charges were used in the subsequent molecular dynamics simulations of three open forms of BRG. As we will discuss, the open forms of BRG came out to be the most relevant forms, and so the extensive integrated approach based calculations were only carried out for these forms. The molecular structures for the open neutral, anionic, and dianionic forms of BRG are shown in Figures 1b, 1c, and 1d, respectively. The 2D chemical drawings and important geometrical parameters for the optimized geometries of open forms of BRG are given in Figure S1 of the Supporting Information. As can be seen the geometrical parameters for the bonds connected to the central carbon are altered significantly depending on the specific form namely neutral, anionic, and dianionic. It is also worth noting that the CO bond length tends to become smaller in the charged forms when compared to the neutral form which suggests the change from single-bond character to double-bond like character of this group. Within MD, to describe the van der Waals interaction of BRG, we employed the general Amber force-field.<sup>37</sup> For the description of the water solvent, we employed the TIP3P force-field. The simulations were carried out in an orthorhombic box with water as solvent molecules and with the required number of chloride counterions to keep the system neutral. The cell dimension of the simulation box was  $72.6 \text{ \AA} \times 72.1 \text{ \AA} \times 68.8 \text{ \AA}$  containing around 11827 water molecules. In order to bring the system to an appropriate density at ambient condition (300 K and 1 atm pressure), the simulations were carried out in an isothermal-isobaric ensemble. The time step for the integration of equation of motion was kept to be 1 fs, and the total time scale of the simulations was around 8 ns. A cutoff length of 10 Å has been employed for computing the van der Waals and electrostatic interactions. For all simulations, we have used the Amber 11 software.<sup>38</sup> The equilibration runs for all three systems were carried out until the density and total interaction energy reached convergence. The final equilibrated configuration from the molecular dynamics runs for  $\text{BRG}^0$ ,  $\text{BRG}^-$ , and  $\text{BRG}^{2-}$  were used as the input configuration for the Car-Parrinello molecular dynamics<sup>39</sup> within a quantum mechanics-molecular mechanics (QM/MM) framework.<sup>40,41</sup> We have described only the BRG solute as the QM region, while the solvents and chloride ions (in the case of anionic and dianionic forms) were included in the MM region. In the hybrid QM/MM-MD, the interaction between the solute and solvents were treated using an effective Hamiltonian approach which accounts for van der Waals and electrostatic interactions between the QM and MM subsystems. This leads to the polarization of the QM subsystem

by the MM charges. Such polarization effects are not taken into account in the standard force-field molecular dynamics simulations. We have used the exchange-correlation functional BLYP<sup>42,43</sup> to describe the QM subsystem. In electronic structure calculations like ours involving plane wave basis sets the number of basis functions (or plane waves) are dictated by the energy cutoff. For that we have chosen a cutoff energy of 80 Ryd. The potential realized by the valence electrons due to the nucleus and core electrons are described through a pseudopotential located on the atomic centers. The use of pseudopotential reduces computational cost significantly since only the valence electrons are described explicitly using the plane waves. The time evolution of the quantum system is dictated by the gradients of Kohn–Sham energies of the QM systems, while the MM system evolves according to the forces computed using classical force-field. The chosen step for integrating the equation of motion was 5 au. The QM/MM simulations are carried in the following order: (i) quenching run (to bring the QM system to the minimum in the Born–Oppenheimer potential energy surface), (ii) scaling run (to bring the system temperature to room temperature), and (iii) Nose run (the system is connected to the Nose thermostat and the simulation is carried out in a canonical ensemble). The total time scale for the production run was around 30 ps in all three cases namely, neutral, anion, and dianion. The trajectories were stored for further analysis of the molecular structure and the solvation shell structure and for carrying out the optical property calculations.

**2.2. Modeling the Optical Properties.** **2.2.1. Static Calculations.** The optimized molecular geometries of BRG<sup>0</sup>, BRG<sup>-</sup>, and BRG<sup>2-</sup> in both open and closed conformation in water solvent have been used as the input structure for calculating the excitation energy using time-dependent density functional theory. We have used both B3LYP and CAM-B3LYP<sup>44,45</sup> levels of theory and TZVP basis set in these calculations.<sup>46</sup> The solvent effect was incorporated using the polarizable continuum model. As mentioned before, the cavity of BRG in the solute was described using an UAHF set. In particular, the use of TZVP basis set for excited state property calculations has been tested many times and has been often recommended by us. However, it is necessary to check this for a specific systems studied, and so we have carried out calculations of excitation energies for the optimized geometries of anionic and dianionic forms of BRG using a number of basis sets with and without including polarization and diffuse functions. The bench-marking involved Pople type basis sets and those developed by Ahlrichs and co-workers<sup>46</sup> and included a number of basis functions in the range 555–1113. Table S1 in the Supporting Information shows excitation energies and oscillator strengths calculated for BRG<sup>-</sup> and BRG<sup>2-</sup> for various basis sets. As can be seen, the TZVP basis set gives results similar to the Def2TZVP basis set but with an additional gain due to reduction in computational cost. From these analysis, it is clearly established that the use of the TZVP basis set for the one photon property calculations for BRG is shown to be pragmatic since it gives the results similar to the Def2TZVP basis set but at the use of less computational cost.

**2.2.2. Dynamic Calculations.** As will be discussed in the next section, based on the static calculations for absorption properties, only the open (neutral, anionic, and dianionic) forms have been identified to be the relevant molecular structures for the pH dependent optical properties of BRG, and so the computationally demanding dynamic averaging of the

property over various configurations was restricted to these systems. Three sets of dynamic calculations were carried out for 100 configurations extracted from the hybrid QM/MM molecular dynamics. All three employ linear response time-dependent density functional theory for obtaining the excitation energies of BRG. However, the description used for describing the environment is different in these sets namely (i) the polarizable continuum model (PCM), (ii) the semicontinuum model (SCM), and (iii) the polarizable electronic embedding (PEE) scheme. The former one describes the solvent as a polarizable continuum, and so accounts for the electrostatic and mutual polarization interaction between the solute–environment subsystems. However, it does not account for hydrogen bonding and charge transfer interactions between the solute and hydrogen bond making polar solvents which is accounted effectively in the SCM approach where the solvent molecules involved in the hydrogen bonding are explicitly included in the QM region. The third approach, which is a recent development for computing the optical properties of chromophores embedded in a solvent or in a heterogeneous environment, employs an effective Hamiltonian to account for the interaction between the solute and the medium. It accounts for electrostatic and polarization interactions between the subsystems. In the former case, the solvent has been described using its macroscopic dielectric parameters, while in the latter approach the solvents are described using classical charges and polarizabilities. The charges in the MM sites polarize the QM system, and so the solute polarization is accounted for. Similarly, the polarizabilities on the MM sites are used to describe the solvent polarization by the solute, and the PEE scheme describes the mutual polarization between the solute and solvent subsystems. Detailed discussion about the implementation and about the incorporation of different interactions between the solute–solvent subsystems in the PEE scheme when compared to the polarizable continuum model can be found in refs 31, 32, and 47.

For the calculations using PCM, only the coordinates of BRG and the solute were used, while for the SCM calculations the solvent molecules that are involved in the hydrogen bonding to the solute were also included explicitly. For this we have computed radial distribution function including all atoms of BRG and the center-of-mass distances of the solvents. Usually, the solvent molecules in the first solvation shell are involved in the hydrogen bonding interaction with the solute. However, there is a dynamic switching of solvent molecules in the first and the second solvation shells which is also associated with dynamic breaking and formation of hydrogen bonds between solute and solvent molecules in the first solvation shell. So, we have included all the solvent molecules within the first and second solvation shells explicitly in the semicontinuum based calculations. A detailed discussion about the solvation shell structure of BRG will follow in the next section. However, here we would like to mention that the solvent molecules appearing within a distance of 4.4 Å from the solute atoms are included explicitly in the SCM calculations. In contrast to this, in the case of the PEE scheme, only the solute molecule is described using the density functional level of theory, and the solvent molecules within a cutoff of 15 Å from the center of mass of BRG were included in the MM region. We use a polarizable force-field according to Ahlström<sup>48</sup> to describe the water solvent which contains charges and polarizabilities placed on the atomic centers. Approximately, around 1000 water molecules were included in the MM region. We also carried

**Table 1.** Excitation Energies (in nm) and the Corresponding Oscillator Strengths (Given in Parentheses) for the Six States of Bromocresol Green in Its Different Ionic Forms<sup>a</sup>

excitation	closed			open		
	neutral	anionic	dianionic	neutral	anionic	dianionic
<b>B3LYP/TZVP</b>						
1	278.29 (0.00)	405.55(0.02)	397.86 (0.01)	575 (0.01)	452 (0.43)	533 (0.68)
2	274.16 (0.03)	380.98(0.04)	385.74 (0.01)	512 (0.22)	423 (0.02)	400 (0.02)
3	270.94 (0.04)	354.24 (0.01)	370.07 (0.03)	484 (0.03)	396 (0.02)	392 (0.08)
4	269.17 (0.01)	339.73 (0.01)	360.16 (0.00)	480 (0.23)	394 (0.00)	390 (0.04)
5	266.88 (0.01)	337.67 (0.00)	330.04 (0.00)	465 (0.06)	384 (0.02)	381 (0.01)
6	260.65 (0.01)	324.02 (0.01)	322.26 (0.00)	426 (0.22)	375 (0.02)	378 (0.02)
<b>CAM-B3LYP/TZVP</b>						
1	252.12 (0.06)	293.15 (0.10)	294.45(0.06)	452 (0.52)	392 (0.68)	503 (0.81)
2	251.15 (0.04)	289.62 (0.01)	293.21(0.06)	403 (0.05)	342 (0.00)	337 (0.27)
3	239.02 (0.00)	288.65 (0.03)	290.19(0.06)	398 (0.22)	330 (0.02)	328 (0.00)
4	238.85 (0.00)	272.16 (0.01)	288.71(0.05)	382 (0.02)	307 (0.10)	321 (0.02)
5	235.39 (0.05)	265.83 (0.04)	285.37(0.10)	366 (0.02)	299 (0.06)	307 (0.00)
6	231.81 (0.00)	251.25 (0.03)	269.84(0.02)	358 (0.13)	293 (0.04)	300 (0.01)
expt						
acidic pH	442					
basic pH	613					

<sup>a</sup>The shown results are from the static approach.

out an additional set of calculations by including two water molecules (which are involved in hydrogen bonding with hydroxyl group of BRG) explicitly in the QM region along with the solute and remaining solvent molecules in MM region. Since the solvent molecules are included explicitly within the QM region this model also accounts for the intermolecular charge transfer between the solute and solvents which may be an important effect when the solute molecules are charged as in the present case (particularly in the case of  $\text{BRG}^-$  and  $\text{BRG}^{2-}$ ). So this set of calculations was carried out only for the anionic and dianionic forms, and the results will be compared later to the case where the solvents are not included explicitly in the QM region. The excitation energies of the BRG solutes were computed as the poles of the linear response function implemented within a TD-DFT/MM framework. The oscillator strengths were obtained as the first residue of the linear response function. We have employed the CAM-B3LYP exchange correlation functional and the TZVP basis set in the calculation of excitation energies and oscillator strengths.

### 3. RESULTS AND DISCUSSIONS

**3.1. Static Results.** The results based on the static approach can provide useful information when the molecules are fairly rigid and exist in a single conformation. However, molecules that can exist in different conformational states pose problems to the computational modeling approach and require that each of them is studied separately with their contributions to the properties being Boltzmann weighted. As we have discussed, BRG can exist in both open and closed forms. The major structural difference between the open and closed forms is due to the hybridization of the central carbon where in the former case it is  $\text{sp}^2$  hybridized, while in the latter case it is  $\text{sp}^3$  hybridized. In addition, each can exist in neutral, anionic, and dianionic forms which are molecular forms that are responsible for the pH dependent optical properties. Though experimentally there are extensive studies on the pH dependent optical properties of BRG, it is not clear which of the forms are responsible.<sup>49,50</sup> Moreover, the energies of the open and closed forms of neutral BRG differ only by 7 kcal/mol (the closed

form is the most stable one) suggesting that any of the forms cannot be excluded based on the energetics. So, it is important to carry out the property calculations for all six forms to find out the most relevant forms when it comes to the pH dependence of the properties. We have therefore optimized all forms (six in total) in water solvent and computed the absorption spectra using the response function formulation of time dependent density functional theory and by using the PCM model for the water solvent. The results for the lowest six excited states are listed in Table 1. Furthermore the excitation energies calculations were carried out using two different levels of theory namely B3LYP and CAM-B3LYP where the latter one has shown efficient performance for modeling optical properties of the systems that involve intramolecular and intermolecular charge transfer. The results, presented in Table 1, reveal that the absorption maximum for open structures are redshifted when compared to closed structures which easily can be attributed to the  $\text{sp}^2$  hybridization of the central carbon in the former case. This allows extended conjugation and causes a redshift of the absorption maximum. The improper dihedral angle (defined between C0–C1–C2–C3 where C0 is the central carbon atom and the remaining are three aromatic carbon atoms bonded to this) computed for the central carbon in the case of neutral structure of closed and open forms are respectively,  $-28.8$  and  $0.5$  degrees. Moreover, the angles between C1–C0–C2, C1–C0–C3, and C2–C0–C3 are around  $109^\circ$  for the former case, while they are increasing to  $120^\circ$  in the latter case. These structural parameters are based on the optimized geometry of the open and the closed forms in water as solvent. In the case of closed structures, the tetrahedral geometry of the central carbon inhibits the electron flow from one phenyl ring to another and so the conjugation. Based on the B3LYP level of theory, the absorption maximum for all three forms (i.e., neutral, anionic, and dianionic) of closed molecular structures is in the range of 275–405 nm, while based on the CAM-B3LYP level of theory, the range further reduces to 250–295 nm. In the case of open forms, the absorption wavelength corresponding to the first excitation is in the range 452–575 nm as predicted from the

B3LYP level of theory, while the absorption wavelength range as predicted from the CAM-B3LYP level of theory is 392–503 nm. It is also worth noticing that the closed forms have smaller oscillator strengths for all transitions when compared to the open forms. The absorption wavelengths predicted for  $\text{BRG}^-$  and  $\text{BRG}^{2-}$  by T. D. Meyer et al. were respectively 463 and 530 nm which are comparable to the values 452 and 533 nm reported in Table 1. The differences seen in these two sets have to be attributed to the use of different basis sets. The experimental absorption wavelength for BRG, with variation in pH, covers the range 445–613 nm and suggests that the open forms of BRG are responsible for its pH dependent behavior. So, a detailed analysis based on the integrated approach is only considered for the open forms. First, we have analyzed the molecular structure and solvation shell structure of the three forms, and then finally we will discuss their optical properties.

**3.2. Dynamic Results.** We have computed various structural parameters for all three protonated forms namely neutral, anionic, and dianionic to find out which set (among neutral/anionic, neutral/dianionic, and anionic/dianionic) can be attributed to the pH dependent optical properties of BRG. In particular, the improper dihedral angle (referred to as  $\phi_0$ ) for the central carbon ( $C_0$ ) connecting the three phenyl rings and the relative orientation of all three phenyl rings (referred to as  $\phi_1$ ,  $\phi_2$ , and  $\phi_3$ ) and bond lengths of the carbons connected to  $C_0$  were analyzed. By looking into the geometry, one can easily understand that BRG is a highly strained system, and that there are different interactions working in favor and against the planarization of it. In particular, the conjugation of the phenyl rings should stabilize the planar conformation, while the steric interactions between ortho-groups of phenyl rings will work against this. So, the molecular conformation of the BRG is established as a compromise between both of these energetic contributions. The dihedral angles  $\phi_1$ ,  $\phi_2$ , and  $\phi_3$  should have values around zero for the planar conformation of the three aromatic moieties, respectively, and they should have  $90^\circ$  for the fully twisted conformer. Moreover, since the  $C_0$  carbon has  $\text{sp}^2$  hybridization, one of the  $C_0-\text{C}_x$  bonds should have double bond character, while the remaining bonds may have single bond character. So, it is also worthwhile looking into any relationship between the bond lengths,  $C_0-\text{C}_x$ , and the corresponding dihedral angles,  $\phi_1$ ,  $\phi_2$ , and  $\phi_3$  (see Figure 2). The computed  $\phi_0$  show a distribution of angles around zero degrees for all three forms suggesting that the central carbon and the three connected carbons are in near-planar geometry, and during the simulation they maintain  $\text{sp}^2$  hybridization. We have also computed the average  $\phi_1$ ,  $\phi_2$ , and  $\phi_3$ , and the values are listed in Table 2. As can be seen the phenyl group connected to the  $\text{SO}_4^{2-}$  group is the most twisted one among all three aromatic groups. It is also worth noticing that when one of the angles  $\phi$  tends to be closer to zero degrees, the other tends to increase toward  $90^\circ$  causing planarity and twistedness of different phenyl rings, respectively. We have also looked for any possible correlation between the dihedral angles,  $\phi_1$ ,  $\phi_2$ , and  $\phi_3$  and the bond length character for the bonds  $C_0-\text{C}_x$  ( $x$  referring to 1, 2, and 3). Due to the increased conjugation,  $C_0-\text{C}_x$  should have more double bond character with these dihedral angles approaching zero. In Figure 3, we show  $\langle R_{\text{C}_0-\text{C}_x}(\phi) \rangle$  versus the three dihedral angles. A clear trend can be seen where the bond length value decreases with angles approaching zero degrees. This is observed for all three cases of neutral, anionic, and dianionic forms of BRG. There appears to be some linear relationship between the average bond length

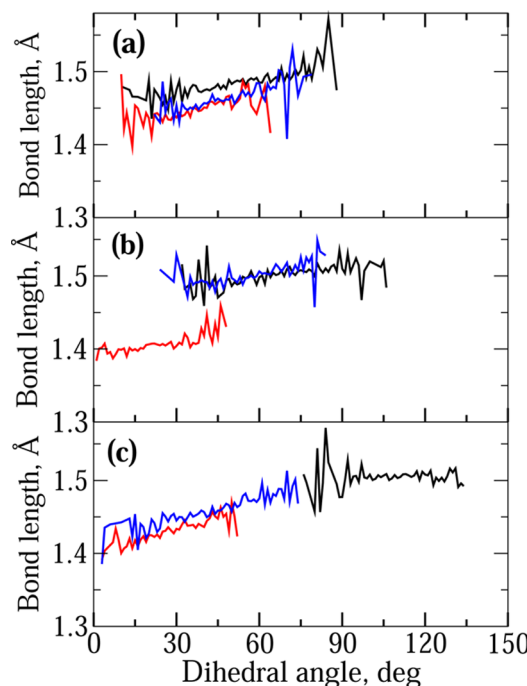


**Figure 2.** Relationship between bond length and dihedral angles,  $\phi$  for open (a) neutral, (b) anionic, and (c) dianionic form of BRG.

**Table 2. Average Structural Parameters and Number of Molecules in Solvation Shells for the Three Open Forms of BRG**

property	system		
	neutral	anionic	dianionic
Average Dihedral Angles, deg			
$\phi_1$	50	36	47
$\phi_2$	69	21	58
$\phi_3$	108	29	43
Solvent Molecules in Different Shells			
shell-1	1.8	0.8	0
shell-2	22.0	22.0	22.8
shell-3	72.5	71.0	70.0

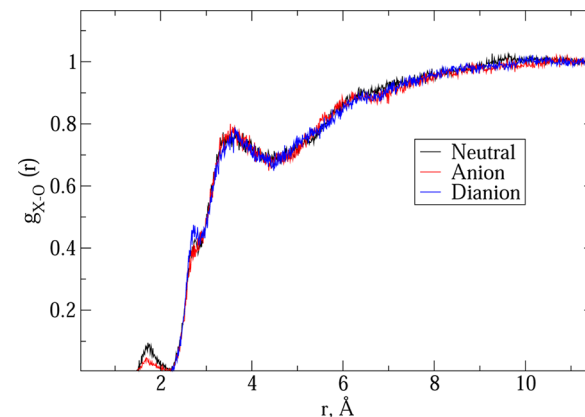


**Figure 3.** Radial distribution function,  $g(r)$  vs the distance,  $r$ , for the neutral, anionic, and dianionic forms of BRG.

and the dihedral angle value. The linear relationship is less pronounced in the case of the anionic form and also for the cases where the dihedral angle value is around  $90^\circ$ .

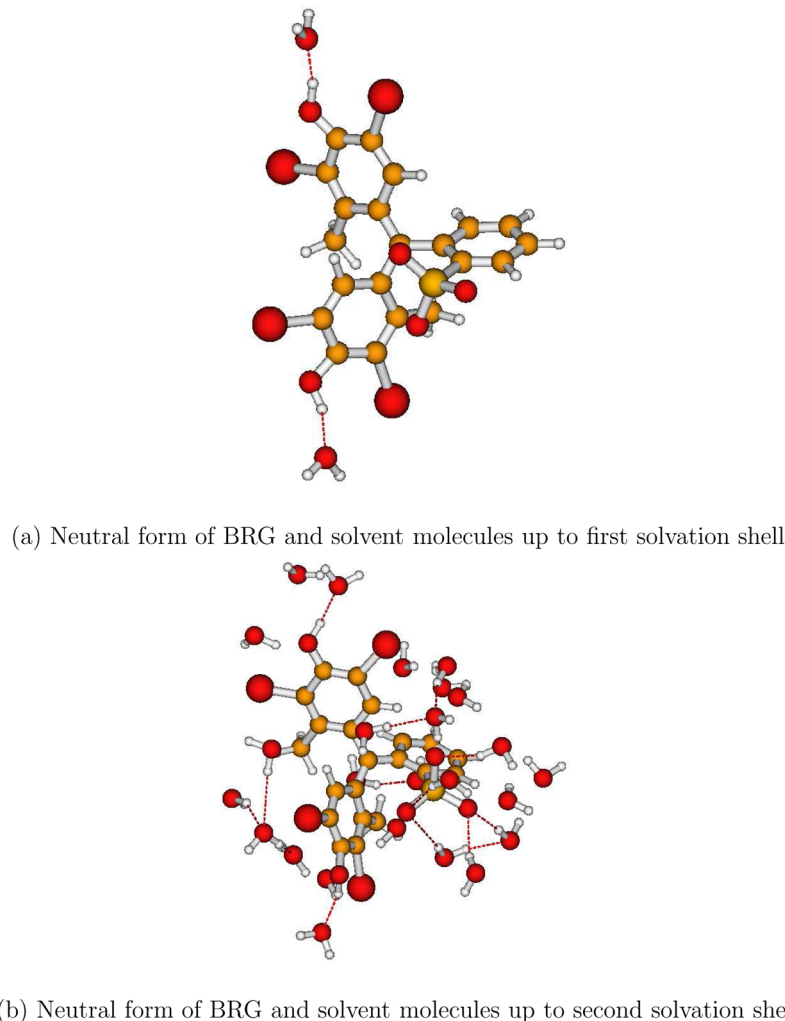


**Figure 4.** Solvation shell structure of the open form of BRG (a) for the first solvation shell of the neutral form and (b) in addition for the second solvation shell of the neutral form.

We will now discuss about the solvation shell structure for  $\text{BRG}^0$ ,  $\text{BRG}^-$ , and  $\text{BRG}^{2-}$ . The three forms differ not only with respect to protonation states but also with respect to their total charge. This might lead to significant differences in the solvation shell structure of different forms which in turn might contribute to the differences in their optical properties. To explore this we have computed the solute-all-atoms and the solvent center-of-mass radial distribution function (rdf) for all three forms. The results are shown in Figure 4. The solvation shell structure seems to have distinct features specific to  $\text{BRG}^0$ ,  $\text{BRG}^-$ , and  $\text{BRG}^{2-}$ . The rdf for the neutral form is characterized by three different peaks. They appear in the distance ranges  $r < 2.2 \text{ \AA}$ ,  $2.2 < r < 3.0 \text{ \AA}$ , and  $3.0 < r < 5.0 \text{ \AA}$ . As we have reported in our earlier studies<sup>51,52</sup> the first solvation shell appears due to hydrogen bonding between the hydroxyl-hydrogen atoms of BRG with oxygen atoms of the water solvent. It is worth noticing that there are two such hydrogen atoms in the case of the neutral form and only one in the anionic form, and none in the case of the dianionic form of BRG. So, the peak height corresponding to the first solvation shell gradually decreases when going from the neutral to the anionic form and disappears for the dianionic form. The trend is reversed in the case of the second solvation shell where the dianionic form is the one associated with a larger peak height. This has to be attributed to

the increased accumulation of charge and for the tendency to keep a larger solvent density. Beyond the second solvation shell there are no significant differences in the solvation shell structure corresponding to different protonation forms. Representative snapshot configurations for the neutral form of BRG with its first solvation shell and second solvation shell are shown in Figures 5a and 5b. The average number of solvent molecules in the first and second solvation shells of BRG are listed for its different protonation forms in Table 2. As can be seen 90% of the time both hydroxyl groups of neutral form are bound to water solvent, while 80% of the time the hydroxyl group of anionic form is bound with water.

Finally, we will discuss the optical properties of different protonated forms of open BRG. The results obtained as averages of various configurations extracted from hybrid QM/MM MD are listed in Table 3. In particular, the results based on solvents described using the implicit and explicit approaches and for vacuum environment are shown. Moreover, the computed absorption spectra for  $\text{BRG}^0$ ,  $\text{BRG}^-$ , and  $\text{BRG}^{2-}$  are shown in Figure 5. The procedure to obtain the spectra has been described in our previous works, and here we explain it briefly.<sup>47</sup> The full spectra is obtained by convoluting the bands corresponding to a few (in the present case it is six) low energy excitations. In order to fit Gaussian to each band we need to

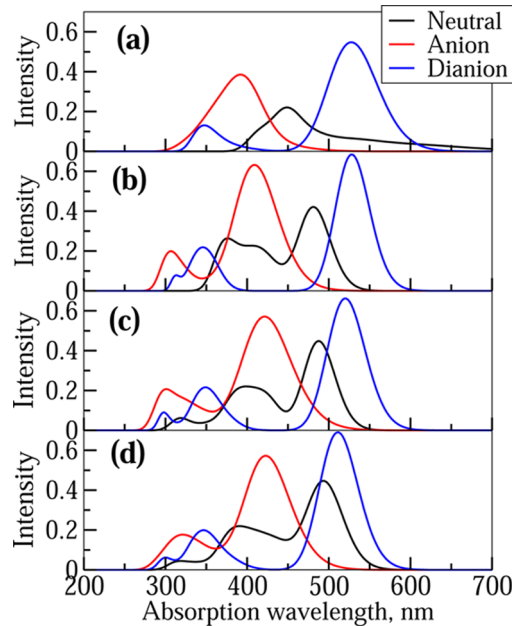


**Figure 5.** Absorption spectra of the neutral, anionic, and dianionic form of BRG calculated by means of the sequential Car–Parrinello hybrid QM/MM molecular dynamics and TD-DFT approach. Excitation energies have been calculated by means of TD-DFT (with CAM-B3LYP functional) using different approaches to describe solvent effect. (a) No solvent effect included, (b) polarizable continuum model, (c) semicontinuum (only solvent molecules up to second solvation shell included explicitly and a continuum model is used to account for the effect due to remaining solvents), and (d) molecular mechanics force-field to describe the solvent effect as implemented in polarizable electronic embedding scheme.

have average absorption wavelength and standard deviation in excitation energies corresponding to a specific excitation. Since we have computed the excitation energies for many configurations (in the present case it involves 100 configurations), it is possible to estimate these two parameters. Further, the average oscillator strength is used to define the amplitude for the Gaussian. So for each excitation a Gaussian can be obtained using the three parameters, and finally the full spectra are obtained by convoluting these Gaussians; and as can be seen this procedure does not involve any empirical parameters. It is worthwhile recalling that for the acidic pH the absorption spectra of BRG is characterized by a single strong band having an absorption maximum ( $\lambda_{\max}$ ) at 442 nm.<sup>49,50</sup> In the basic pH condition, the absorption spectra are rather characterized by two bands with the intense band having  $\lambda_{\max}$  at 613 nm, while for the second band it is situated at 400 nm.<sup>49,50</sup> So, when going from acidic pH to basic pH the absorption maximum of BRG is redshifted by 171 nm, and this is also associated with a 2-fold increase in the intensity of the first band. There are three possibilities of the interconversion process to explain the optical behavior of BRG when the pH condition changes from acidic to basic: (i) neutral  $\Rightarrow$  anionic, (ii) neutral  $\Rightarrow$  dianionic, and (iii) anionic  $\Rightarrow$  dianionic. The other possibilities are excluded because the acidic-pH molecular form should be protonated when compared to the basic-pH molecular form of the BRG molecule. A closer look into the computed absorption spectra based on different solvent models suggests that the anionic and dianionic forms of BRG are responsible for its pH dependent behavior. The neutral  $\Rightarrow$  anionic interconversion yields rather a blueshift in the

**Table 3.** Six Low Energy Excitations (in nm) and the Corresponding Oscillator Strengths (Given in Parentheses) for Bromocresol Green in Its Different Ionic Forms<sup>a</sup>

excitation	neutral	anionic	dianionic
<b>MM-0</b>			
1	820.6 (0.003)	445.0 (0.025)	527.7 (0.548)
2	605.1 (0.032)	400.6 (0.276)	381.9 (0.023)
3	529.6 (0.046)	379.0 (0.117)	358.0 (0.061)
4	475.6 (0.080)	364.1 (0.087)	347.6 (0.052)
5	447.9 (0.166)	350.9 (0.057)	339.8 (0.030)
6	417.0 (0.099)	331.4 (0.050)	333.5 (0.025)
<b>PCM</b>			
1	482.18 (0.42)	410.61 (0.63)	528.97 (0.68)
2	427.79 (0.12)	359.12 (0.03)	355.37 (0.14)
3	410.93 (0.10)	343.98 (0.02)	343.22 (0.08)
4	396.21 (0.07)	323.57 (0.09)	334.08 (0.06)
5	383.44 (0.08)	311.06 (0.05)	324.07 (0.03)
6	370.15 (0.07)	301.56 (0.05)	311.63 (0.02)
<b>Semicontinuum</b>			
1	484.31 (0.47)	423.53 (0.57)	521.31 (0.66)
2	426.68 (0.08)	365.47 (0.03)	375.08 (0.06)
3	408.46 (0.08)	343.83 (0.07)	356.70 (0.10)
4	384.12 (0.18)	327.25 (0.07)	340.99 (0.15)
5	349.96 (0.04)	314.45 (0.08)	311.70 (0.03)
6	318.76 (0.02)	297.11 (0.06)	297.39 (0.03)
<b>MM-2</b>			
1	494.1 (0.441)	423.1 (0.570)	511.2 (0.691)
2	439.4 (0.113)	370.5 (0.046)	376.8 (0.052)
3	411.0 (0.110)	344.2 (0.073)	351.7 (0.142)
4	382.6 (0.183)	326.4 (0.083)	334.0 (0.100)
5	338.6 (0.035)	311.9 (0.089)	311.5 (0.022)
6	312.2 (0.030)	295.7 (0.053)	298.2 (0.052)
<b>Expt</b>			
acidic pH	442		
basic pH	613		

<sup>a</sup>The shown results are from different dynamic approaches.

absorption spectra (refer to Figure 5) suggesting that this interconversion process can be excluded as a possibility to explain the pH dependent optical properties in BRG. Interestingly, neutral  $\Rightarrow$  dianionic interconversion yields a redshift, but the values are much smaller when compared to the experimental value; and so this interconversion process also has been excluded as the responsible mechanism to explain the pH dependence of optical properties of BRG. Only the anionic  $\Rightarrow$  dianionic conversion appears to reproduce the experimental redshift in the absorption spectra and the spectral features of BRG in different pH ranges. The redshifts calculated by means of MM-0, continuum, semicontinuum, and PEE approaches are 83, 118, 97, and 88 nm, respectively. They are smaller clearly than the experimental redshift of 171 nm. Among all four models the results based on the polarizable continuum model are comparably the best. It is interesting to notice that the results based on the semicontinuum and PEE approach are not better than the continuum approach based results. This is rather striking since all the calculations are carried out in water, a more polar solvent where the semicontinuum models are supposed to perform better. Obviously the optical properties of the pH probes are dominated by the protonated and nonprotonated molecular forms, respectively, and so the level of description of the solvent may not be that important. This behavior of pH probes is quite different compared to

solvatochromic probes where the quantitative estimate of the solvatochromic shift requires a better solvent description such as that used in the semicontinuum or hybrid QM/MM response approaches.<sup>47,53</sup> Since the anionic and dianionic forms are charged, we have also carried out a set of calculations within the PEE scheme where the solvents involved in hydrogen bonding with solute are included in QM region. The computed spectra for these two forms compared to the case where all the solvents were included in MM region are shown in Figure S2 of the Supporting Information. As can be seen, the spectra are similar suggesting that the intermolecular charge transfer between the solute and solvents does not alter the shape and peak positions of the spectra significantly.

We have also analyzed the nature of the excitation associated with larger oscillator strength. In the case of the anion, the first intense band has a larger HOMO $\Rightarrow$ LUMO character. The molecular orbitals involved in the excitation are shown in Figures 6a and 6b. In the HOMO molecular orbital, the

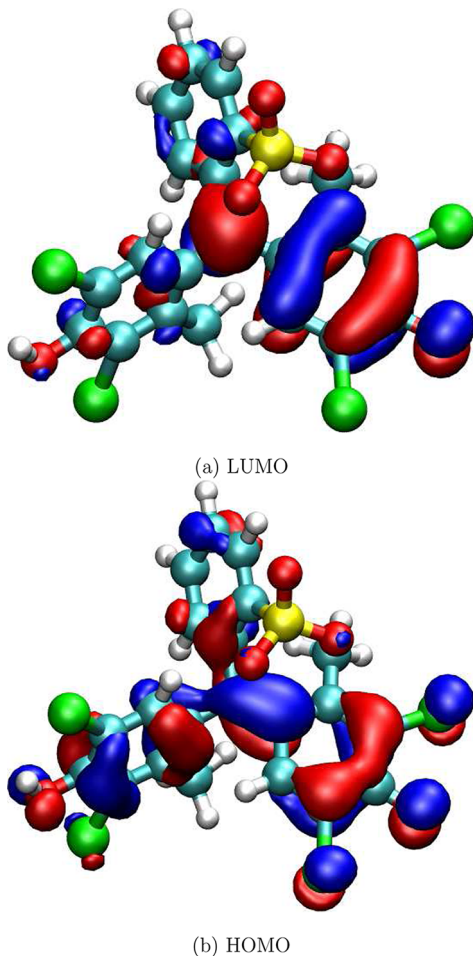


**Figure 6.** Frontier molecular orbitals (HOMO and LUMO) involved in the first intense excitation of anionic BRG.

electron density is delocalized on the aromatic rings connected to bromide atoms. In the LUMO molecular orbital, the charge density is mostly localized on the central carbon and a phenyl group with connected to the  $\text{SO}_4^{2-}$  group. The excitation appears to involve depletion of electron density from the bromide and hydroxyl groups (and so has some intramolecular charge transfer character). Similarly, in the case of the dianionic form the excitation involves some charge transfer from the two

phenyl rings (connected to bromide atoms) to the phenyl ring connected to the  $\text{SO}_4^{2-}$  group. The second intense band is associated with the excitation having  $\text{HOMO}-1\Rightarrow\text{LUMO}$  character. The frontier molecular orbitals involved in the first and second intense excitation are shown in Figures 7 and 8, respectively.

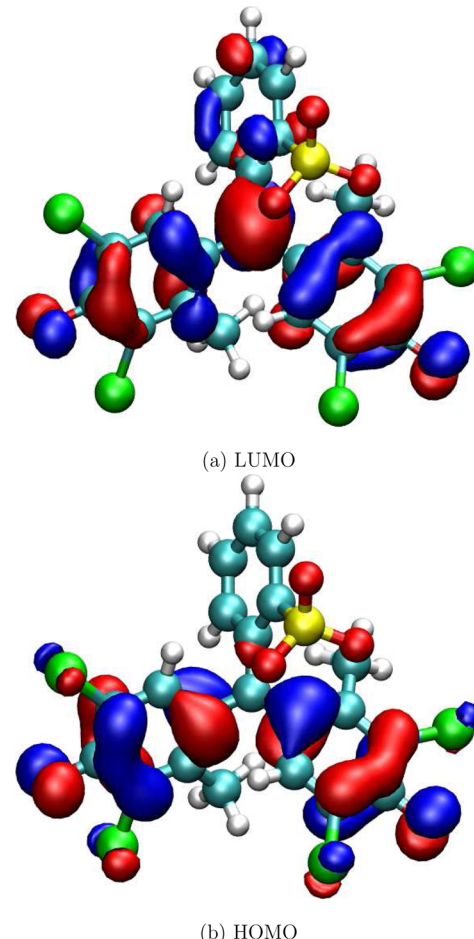


**Figure 7.** HOMO and LUMO orbitals for the dianionic form.

**3.3. Conclusions.** Bromocresol green is a well-known probe used in the quantitative estimation of pH and drug molecules, and biomolecules like albumin and alkalinity. It is used in a number of applications related to diagnosis and water treatment. However, there is still only limited understanding of the mechanism underlying sensitivity of the optical signal of the molecule to external parameters like pH, alkalinity, and dielectric nature of a microenvironment. In this work we have investigated the molecular forms that are responsible for pH dependent optical properties of BRG using static and integrated molecular modeling approaches. Open and closed forms of BRG in their three protonation states were considered as the candidate molecular structures for the static approach. Extensive integrated Car–Parrinello molecular dynamics and time dependent density functional theory within solvents described using different levels of theory has been used to study the most relevant molecular structures, namely the neutral, anionic, and dianionic structures of the open form. The molecular geometry and in particular the conformational nature of the different aromatic rings, the solvation shell structure, and the optical properties for all three forms have been analyzed in

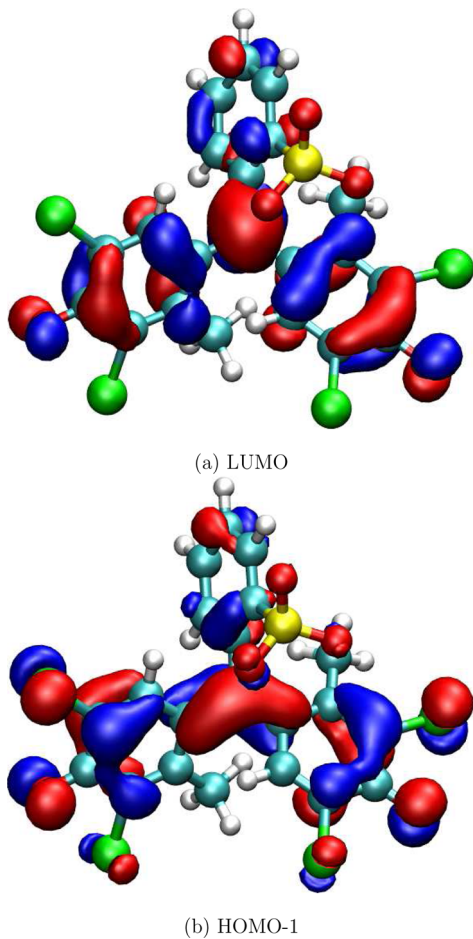


**Figure 8.** HOMO and LUMO orbitals for the dianionic form.

detail. Based on the spectral features of the anionic and dianionic forms and the redshift corresponding to the anionic $\Rightarrow$ dianionic transition which is in good agreement with experimental reports, it is proposed that these anionic and dianionic forms are responsible for the pH dependent optical properties of BRG. This report demonstrates that much can be understood about the working mechanism of pH probes and that design principles can be established from modern molecular modeling approaches.

## ASSOCIATED CONTENT

### Supporting Information

Supporting information includes Table S1 and Figures S1 and S2. Table S1 shows excitation energies and oscillator strengths for anionic and dianionic forms obtained using different basis sets. Figure S1 displays 2D chemical drawings and important geometrical parameters for the open neutral, anionic and dianionic forms of BRG. Figure S2 displays the absorption spectra for anionic and dianionic forms of BRG using hybrid QM/MM approaches with and without explicit water molecules. This material is available free of charge via the Internet at <http://pubs.acs.org>.

## AUTHOR INFORMATION

### Corresponding Author

\*E-mail: murugan@theochem.kth.se.

### Notes

The authors declare no competing financial interest.

## ACKNOWLEDGMENTS

This work was supported by a grant from the Swedish Infrastructure Committee (SNIC) for the project “Multiphysics Modeling of Molecular Materials”, SNIC 023/07-18.

## REFERENCES

- Wencel, D.; Abel, T.; McDonagh, C. Optical Chemical pH Sensors. *Anal. Chem.* **2014**, *86*, 15–29.
- Lin, J. Recent Development and Applications of Optical and Fiber-Optic pH Sensors. *Trends Anal. Chem.* **2000**, *19*, 541–552.
- Madsen, J.; Canton, I.; Warren, N. J.; Themistou, E.; Blanazs, A.; Ustbas, B.; Tian, X.; Pearson, R.; Battaglia, G.; Lewis, A. L.; Armes, S. P. Nile Blue-Based Nanosized pH Sensors for Simultaneous Far-Red and Near-Infrared Live Bioimaging. *J. Am. Chem. Soc.* **2013**, *135*, 14863–14870.
- Schreml, S.; Meier, R. J.; Wolfbeis, O. S.; Landthaler, M.; Szeimies, R.-M.; Babilas, P. 2D Luminescence Imaging of pH In Vivo. *Proc. Natl. Acad. Sci. U.S.A.* **2011**, *108*, 2432–2437.
- Narayanaswamy, R.; Wolfbeis, O. S. *Optical sensors: industrial, environmental and diagnostic applications*; Springer: 2004; Vol. 1.
- Thomas, J. A.; Buchsbaum, R. N.; Zimniak, A.; Racker, E. Intracellular pH Measurements in Ehrlich Ascites Tumor Cells Utilizing Spectroscopic Probes Generated In Situ. *Biochemistry* **1979**, *18*, 2210–2218.
- Tantama, M.; Hung, Y. P.; Yellen, G. Imaging Intracellular pH in Live Cells with a Genetically Encoded Red Fluorescent Protein Sensor. *J. Am. Chem. Soc.* **2011**, *133*, 10034–10037.
- Wong, W.-M.; Wong, B. C.-Y. Definition and Diagnosis of Gastroesophageal Reflux Disease. *J. Gastroenterol. Hepatol.* **2004**, *19*, S26–S32.
- Zhang, X.; Lin, Y.; Gillies, R. J. Tumor pH and Its Measurement. *J. Nucl. Med.* **2010**, *51*, 1167–1170.
- Tannock, I. F.; Rotin, D. Acid pH in Tumors and Its Potential for Therapeutic Exploitation. *Cancer Res.* **1989**, *49*, 4373–4384.
- Zhang, S.; Rich, A. Direct Conversion of an Oligopeptide from a  $\beta$ -sheet to an  $\alpha$ -helix: A Model for AmyloidFormation. *Proc. Natl. Acad. Sci. U.S.A.* **1997**, *94*, 23–28.
- Shaw, A. K.; Pal, S. K. Spectroscopic Studies on the Effect of Temperature on pH-Induced Folded States of Human Serum Albumin. *J. Photochem. Photobiol., B* **2008**, *90*, 69–77.
- Soto, C. Protein Misfolding and Disease; Protein Refolding and Therapy. *FEBS Lett.* **2001**, *498*, 204–207.
- Smith, D. G.; McMahon, B. K.; Pal, R.; Parker, D. Live Cell Imaging of Lysosomal pH Changes with pH Responsive Ratiometric Lanthanide Probes. *Chem. Commun.* **2012**, *48*, 8520–8522.
- Breland, J. A.; Byrne, R. H. Spectrophotometric Procedures for Determination of Sea Water Alkalinity Using Brom cresol Green. *Deep Sea Res., Part I* **1993**, *40*, 629–641.
- Dennis, A. M.; Rhee, W. J.; Sotto, D.; Dublin, S. N.; Bao, G. Quantum Dot-Fluorescent Protein FRET Probes for Sensing Intracellular pH. *ACS Nano* **2012**, *6*, 2917–2924.
- Medintz, I. L.; Uyeda, H. T.; Goldman, E. R.; Mattoussi, H. Quantum Dot Bioconjugates for Imaging, Labelling and Sensing. *Nat. Mater.* **2005**, *4*, 435–446.
- Berkovic, G.; Krongauz, V.; Weiss, V. Spiropyrans and spirooxazines for memories and switches. *Chem. Rev.* **2000**, *100*, 1741–1754.
- Otto, A. H.; Schrader, S.; Steiger, T.; Schneider, M. Gas-Phase Deprotonation Energies of Sulfuric Acid, Perchloric Acid, Chlorosulfuric Acid and Fluorosulfuric Acid. *J. Chem. Soc., Faraday Trans* **1997**, *93*, 3927–3930.
- Otto, A. H.; Steiger, T.; Schrader, S.  $\text{HAlCl}_4$  in the Gas Phase is Stronger Than  $\text{HTaF}_6$ . *Chem. Commun.* **1998**, 391–392.
- Otto, A. H.; Steiger, T.; Schrader, S. The Gas Phase Acidity of Trifluoromethanesulphonic Acid. An Ab Initio MO and Density Functional Theory Study. *J. Mol. Struct.* **1998**, *471*, 105–113.
- Otto, A. H.; Prescher, D.; Gey, E.; Schrader, S. Proton Affinities of Some Polyfluoroalkanes in Comparison to the Unsubstituted

- Alkanes. The Estimation of the Proton Affinities of Polytetrafluoroethylene and Polyethylene by Applying Theoretical Methods. *J. Fluorine Chem.* **1997**, *82*, 55–71.
- (23) Murugan, N. A.; Kongsted, J.; Ågren, H. pH Induced Modulation of One and Two-photon Absorption Properties in a Naphthalene Based Molecular Probe. *J. Chem. Theory Comput.* **2013**, *9*, 3660–3669.
- (24) Machuqueiro, M.; Baptista, A. M. Constant-pH Molecular Dynamics with Ionic Strength Effects: ProtonationConformation Coupling in Decalsine. *J. Phys. Chem. B* **2006**, *110*, 2927–2933.
- (25) Patnaik, S. S.; Trohalaki, S.; Pachter, R. Molecular Modeling of Green fluorescent Protein: Structural Effects of Chromophore Deprotonation. *Biopolymers* **2004**, *75*, 441–452.
- (26) De Angelis, F.; Fantacci, S.; Selloni, A. Time-Dependent Density Functional Theory Study of the Absorption Spectrum of  $[\text{Ru}(4,4'\text{-COOH-}2,2'\text{-bpy})_2(\text{NCS})_2]$  in Water Solution: Influence of the pH. *Chem. Phys. Lett.* **2004**, *389*, 204–208.
- (27) Steindal, A. H.; Olsen, J. M. H.; Ruud, K.; Frediani, L.; Kongsted, J. A Combined Quantum Mechanics/Molecular Mechanics Study of the One-and Two-Photon Absorption in the Green Fluorescent Protein. *Phys. Chem. Chem. Phys.* **2012**, *14*, 5440–5451.
- (28) Patnaik, S. S.; Trohalaki, S.; Naik, R. R.; Stone, M. O.; Pachter, R. Computational Study of the Absorption Spectra of Green Fluorescent Protein Mutants. *Biopolymers* **2007**, *85*, 253–263.
- (29) Tomasi, J.; Mennucci, B.; Cammi, R. Quantum Mechanical Continuum Solvation Models. *Chem. Rev.* **2005**, *105*, 2999–3094.
- (30) Besley, N. A.; Hirst, J. D. Ab Initio Study of the Electronic Spectrum of Formamide with Explicit Solvent. *J. Am. Chem. Soc.* **1999**, *121*, 8559–8566.
- (31) Olsen, J. M.; Aidas, K.; Kongsted, J. Excited States in Solution through Polarizable Embedding. *J. Chem. Theory Comput.* **2010**, *6*, 3721–3734.
- (32) Olsen, J. M. H.; Kongsted, J. Molecular Properties through Polarizable Embedding. *Adv. Quantum Chem.* **2011**, *61*, 107–143.
- (33) De Meyer, T.; Hemelsoet, K.; Van Speybroeck, V.; De Clerck, K. Substituent Effects on Absorption Spectra of pH Indicators: An Experimental and Computational Study of Sulfonphthaleine Dyes. *Dyes Pigm.* **2014**, *102*, 241–250.
- (34) Frisch, M. J. Trucks, G. W.; Schlegel, H. B.; Scuseria, G. E.; Robb, M. A.; Cheeseman, J. R.; Scalmani, G.; Barone, V.; Mennucci, B.; Petersson, G. A.; Nakatsuji, H.; Caricato, M.; Li, X.; Hratchian, H. P.; Izmaylov, A. F.; Bloino, J.; Zheng, G.; Sonnenberg, J. L.; Hada, M.; Ehara, M.; Toyota, K.; Fukuda, R.; Hasegawa, J.; Ishida, M.; Nakajima, T.; Honda, Y.; Kitao, O.; Nakai, H.; Vreven, T.; Montgomery, J. A., Jr.; Peralta, J. E.; Ogliaro, F.; Bearpark, M.; Heyd, J. J.; Brothers, E.; Kudin, K. N.; Staroverov, V. N.; Kobayashi, R.; Normand, J.; Raghavachari, K.; Rendell, A.; Burant, J. C.; Iyengar, S. S.; Tomasi, J.; Cossi, M.; Rega, N.; Millam, N. J.; Klene, M.; Knox, J. E.; Cross, J. B.; Bakken, V.; Adamo, C.; Jaramillo, J.; Gomperts, R.; Stratmann, R. E.; Yazyev, O.; Austin, A. J.; Cammi, R.; Pomelli, C.; Ochterski, J. W.; Martin, R. L.; Morokuma, K.; Zakrzewski, V. G.; Voth, G. A.; Salvador, P.; Dannenberg, J. J.; Dapprich, S.; Daniels, A. D.; Farkas, Ö.; Foresman, J. B.; Ortiz, J. V.; Cioslowski, J.; Fox, D. J. *Gaussian 09, Revision A.02*; Gaussian, Inc.: Wallingford, CT, 2009.
- (35) Barone, V.; Cossi, M.; Tomasi, J. A New Definition of Cavities for the Computation of Solvation Free Energies by the Polarizable Continuum Model. *J. Chem. Phys.* **1997**, *107*, 3210–3221.
- (36) Breneman, C.; Wiberg, K. Determining Atom-Centered Monopoles from Molecular Electrostatic Potentials. The Need for High Sampling Density in Formamide Conformational Analysis. *J. Comput. Chem.* **1990**, *11*, 361–373.
- (37) Wang, J.; Wolf, R.; Caldwell, J.; Kollman, P.; Case, D. Development and Testing of a General AMBER Force Field. *J. Comput. Chem.* **2004**, *34*, 1157–1174.
- (38) Case, D. A.; Darden, T. A.; Cheatham, T. E.; Simmerling, C. L.; Wang, J.; Duke, R. E.; Luo, R.; Walker, R. C.; Zhang, W.; Merz, K. M.; Roberts, R.; Wang, B.; Hayik, S.; Roitberg, A.; Seabra, G.; Kolossvai, I.; Wong, K. F.; Paesani, F.; Vanicek, J.; Liu, J.; Wu, X.; Brozell, S. R.; Steinbrecher, T.; Gohlke, H.; Cai, Q.; Ye, X.; Wang, J.; Hsieh, M.-J.;
- Cui, G.; Roe, D. R.; Mathews, D. H.; Seetin, M. G.; Sagui, C.; Babin, V.; Luchko, T.; Gusarov, S.; Kovalenko, A.; Kollman, P. A. *Amber 11*; University of California: San Francisco, 2010.
- (39) Car, R.; Parrinello, M. Unified Approach for Molecular Dynamics and Density-Functional Theory. *Phys. Rev. Lett.* **1985**, *55*, 2471.
- (40) Warshel, A.; Levitt, M. Theoretical Studies of Enzymic Reactions: Dielectric, Electrostatic and Steric Stabilization of the Carbonium Ion in the Reaction of Lysozyme. *J. Mol. Biol.* **1976**, *103*, 227–249.
- (41) Field, M. J.; Bash, P. A.; Karplus, M. A Combined Quantum Mechanical and Molecular Mechanical Potential for Molecular Dynamics Simulations. *J. Comput. Chem.* **1990**, *11*, 700–733.
- (42) Becke, A. D. Density-Functional Exchange-Energy Approximation with Correct Asymptotic Behavior. *Phys. Rev. A* **1988**, *38*, 3098–3100.
- (43) Lee, C.; Yang, W.; Parr, R. G. Development of the Colle-Salvetti Correlation-Energy Formula into a Functional of the Electron Density. *Phys. Rev. B* **1988**, *37*, 785–789.
- (44) Yanai, T.; Tew, D. P.; Handy, N. C. A New Hybrid Exchange-Correlation Functional Using the Coulomb-Attenuating Method (CAM-B3LYP). *Chem. Phys. Lett.* **2004**, *393*, 51–57.
- (45) Peach, M. J. G.; Helgaker, T.; Sałek, P.; Keal, T. W.; Lutnæs, O. B.; Tozer, D. J.; Handy, N. C. Assessment of a Coulomb-Attenuated Exchange-Correlation Energy Functional. *Phys. Chem. Chem. Phys.* **2006**, *8*, 558–562.
- (46) Schafer, A.; Huber, C.; Ahlrichs, R. Fully Optimized Contracted Gaussian Basis Sets of Triple Zeta Valence Quality for Atoms Li to Kr. *J. Chem. Phys.* **1994**, *100*, 5829–5835.
- (47) Murugan, N. A.; Kongsted, J.; Rinkevicius, Z.; Aidas, K.; Ågren, H. Modeling the Structure and Absorption Spectra of Stilbazolium Merocyanine in Polar and Nonpolar Solvents Using Hybrid QM/MM Techniques. *J. Phys. Chem. B* **2010**, *114*, 13349–13357.
- (48) Ahlström, P.; Wallqvist, A.; Engström, S.; Jönsson, B. A Molecular Dynamics Study of Polarizable Water. *Mol. Phys.* **1989**, *68*, 563–581.
- (49) Ismail, F.; Malins, C.; Goddard, N. J. Alkali Treatment of Dye-Doped Sol-Gel Glass Films for Rapid Optical pH Sensing. *Analyst* **2002**, *127*, 253–257.
- (50) Makote, R.; Collinson, M. Organically Modified Silicate Films for Stable pH Sensors. *Anal. Chim. Acta* **1999**, *394*, 195–200.
- (51) Murugan, N. A.; Ågren, H. Role of Dynamic Flexibility in Computing Solvatochromic Properties of Dye/Solvent Systems: o-Betaine in Water. *J. Phys. Chem. A* **2009**, *113*, 2572–2577.
- (52) Murugan, N. A.; Jha, P. C.; Rinkevicius, Z.; Ruud, K.; Ågren, H. Solvatochromic Shift of Phenol BBBlue in Water from a Combined CarParrinello Molecular Dynamics Hybrid Quantum Mechanics-Molecular Mechanics and ZINDO Approach. *J. Chem. Phys.* **2010**, *132*, 234508.
- (53) Murugan, N. A. Modeling Solvatochromism of a Quinolinium Betaine Dye in Water Solvent Using Sequential Hybrid QM/MM and Semicontinuum Approach. *J. Phys. Chem. B* **2011**, *115*, 1056–1061.